Study of electron-irradiated silicon thin films using transient photocurrent spectroscopy

2014 J. Phys.: Conf. Ser. 558 012001

(http://iopscience.iop.org/1742-6596/558/1/012001)

Journal of Physics: Conference Series **558** (2014) 012001 doi:10.1088/1742-6596/558/1/012001

Study of electron-irradiated silicon thin films using transient photocurrent spectroscopy

S Reynolds[1], O Astakhov[2] and V Smirnov[2]
[1] School of Engineering, Physics and Mathematics, University of Dundee, Dundee DD1 4HN, Scotland.
[2] IEK-5 Photovoltaik, Forschungszentrum Jülich, D-52425 Jülich, Germany.

E-mail: s.z.reynolds@dundee.ac.uk

Abstract. Electron irradiation of silicon thin films creates localised states, which degrade their opto-electronic properties. We present a series of transient photocurrent spectroscopy (TPC) measurements on electron-irradiated amorphous and microcrystalline silicon films, annealed at progressively increasing temperatures. This has enabled localised states associated with both dangling bonds and conduction band tails to be examined over a wide energy range. Trends in the evolution of the DOS following electron irradiation followed by isochronal annealing steps indicate reductions in the deep defect density, which correlate with spin density. We also find a steepening of the conduction band tail slope in amorphous silicon on annealing. Both defect density and tail slope may be restored close to as-prepared material values. Earlier CPM data are re-examined, and a similar trend in the valence band tail slope is indicated. Computer simulations predict that following e-irradiation changes in deep defect density primarily control solar cell performance, and will tend to obscure effects related to band tails.

1. Introduction

The effects of energetic charged particles on films of hydrogenated amorphous silicon (a-Si:H) [1-4] and microcrystalline silicon (μc-Si:H) [5-10] solar cells and the transport properties of single films [11-16] have been studied extensively, due mainly to potential applications in space PV. It is generally agreed that the predominant effect of radiation damage is to create silicon dangling bonds (DBs), detected as unpaired spins in ESR measurements, which are metastable and can largely be removed by thermal annealing. While there is debate over the detailed process of DB creation [4], the outcome is evidently similar to that of light-induced degradation (Staebler-Wronski effect, SWE) [17]. However higher spin densities, approaching 10^{19} cm^{-3}, can be generated by low-temperature e-irradiation, a figure only reached by light-soaking using pulsed lasers [18] or within small volumes [19].

The effect of increased defect densities on the performance of thin-film silicon solar cells is predominantly a consequence of increased carrier recombination in the absorber layer, which reduces the short-circuit current density J_{SC}, coupled with a reduction in electric field strength in certain regions due to increased trapped space-charge, which degrades the fill-factor *FF*. Reduction in open-circuit voltage V_{OC} is comparatively minor. Remarkably, cells heavily degraded by e-irradiation (J_{SC} < 1 mA/cm^2, *FF* < 30%) may be restored to performance approaching that of a pristine cell by annealing for an hour at 180 °C [7].

As well as improving our ability to predict performance of cells in space applications, defects created by laboratory e-irradiation may be used to gain a more general understanding of solar cell

physics and material limitations. By using annealing steps to control the defect density in the absorber layer, laboratory measurements of solar cell properties, coupled with computer simulations, enable a detailed optoelectronic model and material parameter sets to be developed [8, 9].

Here we investigate the effect of 2 MeV electron fluences of up to 10^{17} cm^{-2} on thin film silicon using transient photocurrent (TPC) density of states (DOS) spectroscopy and ESR spin density measurements following successive 30 min. annealing periods between room temperature and 180 °C. Some earlier constant photocurrent (CPM) measurements are also re-visited. Results are linked to the performance of solar cells with varying defect distributions by computer simulations.

2. Experimental

2.1. Film deposition

Intrinsic thin film silicon layers were prepared by PECVD using optimized conditions [20], and deposited on glass substrates. The chamber pressure, RF power and silane concentration respectively were: a-Si:H samples: 3 mbar, 3 W, 10%; μc-Si:H samples: 1.5 mbar, 20 W, 4.9%. A substrate temperature of 180°C was used throughout. Crystallinity of μc-Si:H absorber layers was determined from Raman measurements.

2.2. e-irradiation and annealing protocols

Films on glass and ESR powder samples underwent identical 2 MeV electron bombardments and subsequent stepwise isochronal thermal annealing procedures. Irradiation was performed at approximately 100K in a liquid nitrogen flow cryostat. Samples were exposed to a beam of 2 MeV electrons with current density 5 $\mu A/cm^2$ for 50 min., giving a fluence of 9.4×10^{16} cm^{-2}. Further details may be found elsewhere [11].

Between the electron bombardment and commencement of the annealing and measurement cycles, samples were transported and stored in liquid nitrogen to prevent uncontrolled annealing of defects. Defect densities in the layers were determined using Electron Spin Resonance (ESR) measurements on a-Si:H and μc-Si:H powder samples [21] deposited under identical deposition conditions to the samples on glass substrates.

Spin densities following successive isochronal annealings are shown in figure 1. Identical annealing regimes were followed, so that ESR spin densities were aligned as closely as possible with the films measured using TPC.

2.3 Transient Photocurrent Spectroscopy

A VSL337 nitrogen laser and dye attachment generates a 3 ns width 620 nm wavelength pulse at the sample, defined by two Ag contacts deposited on the Si film separated by a 1 mm gap, across which a 300 volt dc bias was maintained. An initial carrier density of some 10^{16} cm^{-3} was established by adjusting the pulse intensity using neutral density filters. Following pre-amplification, the photocurrent decay was recorded by a Tektronix TDS3052 oscilloscope. Repetitive averaging was used to reduce the noise to an acceptable level, and the data transferred to a PC for analysis, display and storage [22]. Each TPC current vs. time data file used subsequently to calculate the DOS is obtained from several sets of overlapping measurements (typically five), over progressively increasing time-scales from ns to seconds. Measurements were conducted at several experimental temperatures, typically 130, 160, 220, 250 and 298 K, giving plots of the DOS extending typically from 0.1 eV to 0.7 eV. Successive annealing steps (between 50 °C and 180 °C, in order of lowest temperature to highest temperature) were carried out on the films, followed by TPC measurements in the same cryostat as described above.

The TPC data files were then processed to extract the DOS present after each annealing step. A spectroscopic method was used in which the current-time data firstly undergo discrete Fourier transformation [23, 24] and are then analysed using techniques developed for modulated photocurrent spectroscopy (MPC). Within a multiple-trapping model, the DOS N_{ti} at the i^{th} level, corresponding to

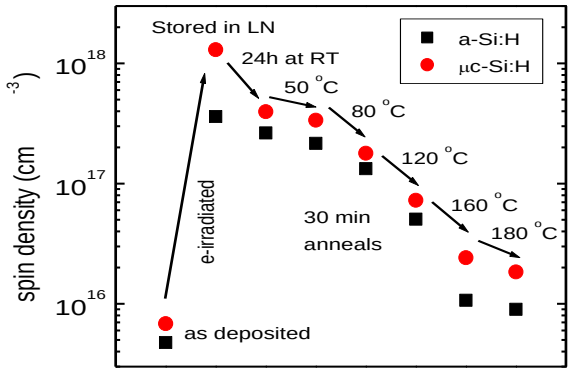

Figure 1. Spin density of a-Si:H and μc-Si:H samples measured after deposition, e-irradiation, transit at liquid nitrogen, 24 h at room temperature, and successive 30 min. annealings.

an energy depth E_ω is

$$N_{ti} \propto \frac{\sin(\phi(\omega))}{C_n |I(\omega)|}, \text{ where } E_\omega = kT \ln(\nu / \omega). \quad (1)$$

Here k is Boltzmann's constant, T the absolute temperature, ν the attempt-to-escape frequency and C_n the carrier capture coefficient. In this derivation C_n and ν are assumed constant for all localized states, and related by detailed balance to the band-edge DOS: $N_C = \nu / C_n$. An attempt-to-escape frequency of 10^{12} s^{-1} combined with an effective band-edge DOS of 10^{20} cm^{-3} was found to offer a suitable overlap between DOS sections measured at different temperatures, and was used throughout this work.

As the spectroscopic method is susceptible to noise, especially at short times, an alternative quantitative analysis is to force-fit the current-time data to the form appropriate for an exponential 'band-tail' of states [25]. Assuming multiple-trapping transport at an experimental temperature T below the conduction band tail temperature T_C, in the 'pre-transit' quasi-equilibrium regime,

$$I(t) \propto t^{-(1-\alpha)}, \quad (2)$$

where the dispersion parameter $\alpha = kT / kT_C$. One may thus obtain α and hence an assumed T_C from fitting a straight line to a log-log plot of the current-time data at short times and low temperatures, where the decay is controlled by band-tail thermalisation prior to the onset of deep trapping or recombination.

2.4 Solar cell simulations

Computer simulation of solar cells was carried out using the *SC-Simul* program developed at the University of Oldenburg. This is a one-dimensional numerical simulation which solves the Poisson equation, the continuity equations for electrons and holes, and the current transport equations including drift, diffusion, and thermionic emission over barriers, if present, in the valence and conduction bands. The thermal equilibrium and steady-state solutions are obtained by Newton iteration. Further details are provided elsewhere [26, 27].

3. Results and discussion

3.1. TPC Spectroscopy – general features

An example of current-time decays for a-Si:H and μc-Si:H at 220 K is shown in figure 2. From similar data recorded at experimental temperatures between 130 K and 360 K, we obtain the spectroscopic DOS plots for a-Si:H and μc-Si:H, shown in figures 3 and 4 respectively, proceeding through the 30 min. annealing steps identified in the legend. In both cases a general trend of decreasing 'integrated'

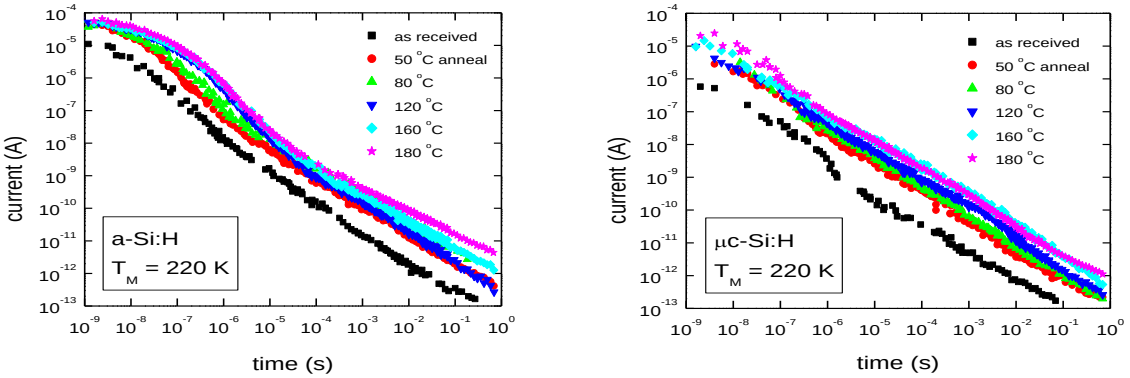

Figure 2. TPC current decay series for a-Si:H and μc-Si:H films measured at 220 K, following annealing of as-received samples for 30 min. at the temperatures indicated.

DOS with increasing anneal temperature is evident. In figure 5 we compare the deep defect density (at 0.5 eV) with the ESR spin density (N_S) data from figure 1. While the data are quite noisy, which may reflect the uncertainties introduced when matching the DOS sections obtained at different temperatures, the relationship is reasonably linear. A similar correlation has been reported previously for the CPM 'defect shoulder' vs. spin density for a-Si:H films, although the situation is less clear for μc-Si:H, with a correlation evident for low crystalline volume fraction films but no general trend for higher volume fractions [11]. Bronner et al [16] have found a systematic reduction in defect density on annealing μc-Si:H films when measured using MPC, although samples could not be returned to their as-deposited condition. Our TPC results therefore largely support previous findings in the case of a-Si:H. Given the rather arbitrary scaling procedure for the TPC DOS, little significance should be attached to the absolute TPC DOS magnitudes.

3.2. Conduction band tails

Switching attention to the shallower states, steepening of the band tail slopes with progressive annealing steps is evident, most clearly for a-Si:H as shown in figure 3. Trends in the μc-Si:H shallow states are less clear; the DOS sections obtained are noisier and overlap with temperature is poorer. An

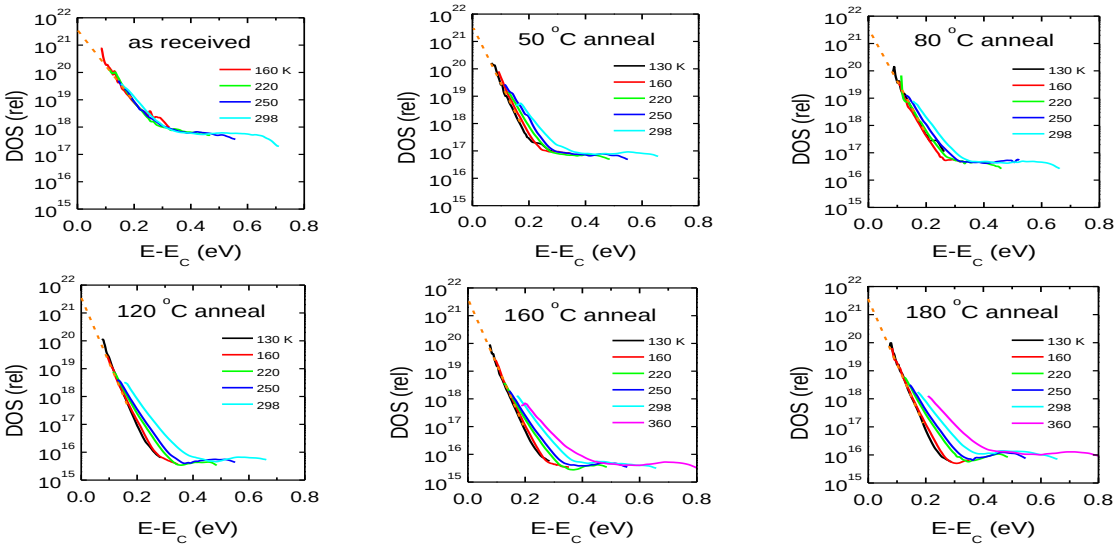

Figure 3. DOS plots for e-irradiated a-Si:H sample, as received and following successive 30 min. anneals. Dashed line is extrapolation to the conduction band edge (assumed 3×10^{21} units).

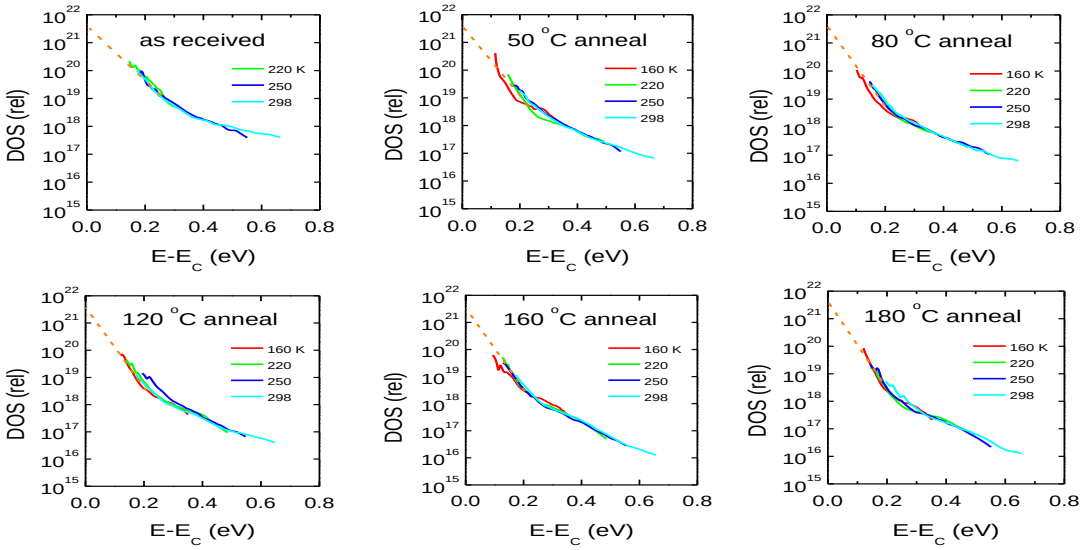

Figure 4. DOS plots for e-irradiated μc-Si:H sample, as received and following successive 30 min. anneals. Dashed line is extrapolation to the band edge (assumed 3×10^{21} units).

alternative measure of the band-tail DOS may be obtained using the force-fit approach defined by equation 2. Figure 6(a) indicates that for a-Si:H the short-time data at low temperatures (160 K data shown) does indeed follow a power law, and the band-tail slopes extracted by this method are plotted in figure 6(b). This confirms the trend evident in the spectroscopic data, and further reveals that the reduction in band-tail slope occurs predominantly after annealing at 120°C with a more gradual reduction between 120 °C and 180 °C.

Apparent inconsistencies in overlap between sections of the DOS in the region of the band tails evident in figure 3 are known to be due to resolution limitations in the MPC DOS method [24]. This becomes more apparent as annealing proceeds and the band tail becomes steeper, where it is only properly resolved below 220 K. The 'envelope' curve formed by the overlapping sections is however, reliable. A general comparison between a-Si:H and μc-Si:H in figures 3 and 4 shows that the band tail slope in the former case is somewhat steeper, in keeping with previous reports [28, 29].

Quantitative changes in CB tail states in a-Si:H following e-irradiation do not appear to have previously been reported explicitly in the literature. There have however been reports of changes in band tail state densities or slopes in a-Si:H following light soaking. Longeaud et al [30] and Roy et al

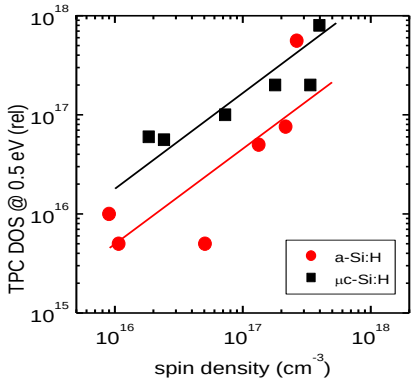

Figure 5. Correlation between relative TPC DOS at 0.5 eV and spin density N_S for a-Si:H and μc-Si:H samples. Lines correspond to an assumed linear relationship between N_S and DOS, with each positioned to provide a best fit.

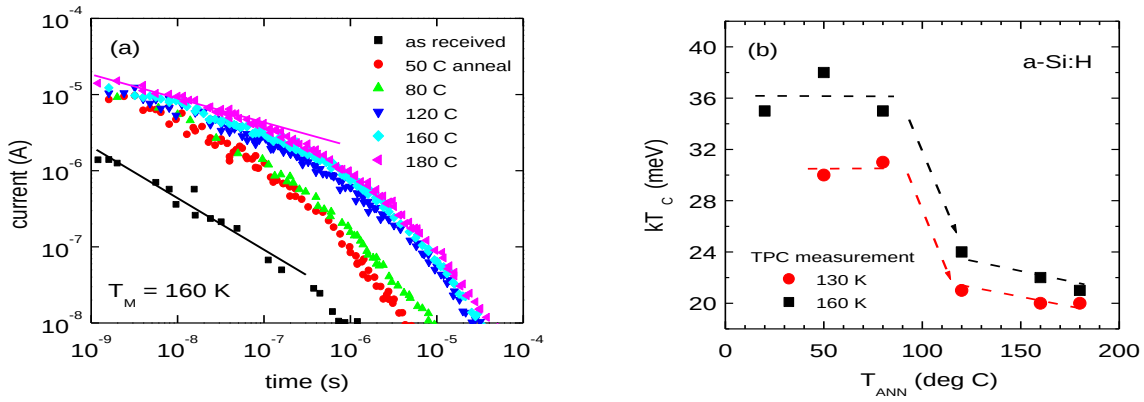

Figure 6. (a) Short-time TPC current decays for a-Si:H film measured at 160 K, following progressive annealing of as-received samples for 30 mins. as indicated. (b) Conduction band tail slopes calculated from best-fit lines as described in the text, *vs.* annealing temperature.

[31] carried out MPC measurements following increasing periods of light illumination, and found that above a certain exposure threshold, increased densities of CB tail states were created. However, in contrast to our results, the changes they report in CB tail states created above the exposure threshold could *not* be annealed out.

Band tails arise from intrinsic disorder in the amorphous structure, with distortions of the bond lengths and angles of tetrahedral coordination frozen-in as a consequence of the deposition process. The implication is therefore that in addition to creating a high density of DBs, electron irradiation introduces greater disorder, or modifies the existing disorder, in a manner which broadens the CB tail.

3.3. Constant Photocurrent Method and Valence Band Tail

TPC spectroscopy enables the DOS of unoccupied artifact states, above the Fermi level, to be examined. In order to probe *occupied* states in undoped a-Si:H, other techniques such as the constant-photocurrent method (CPM), are required. The CPM optical absorption spectrum $\alpha(E_P)$ integrates transitions in which electrons in filled localised states absorb the photon energy E_P and enter transport states above the CB mobility edge E_C. The term $d\alpha/dE_P$ is thus proportional to the DOS at $(E_C - E_P)$ [32]. Other transitions are also possible, but probably contribute little here. We have used CPM data from a previous publication [12] to construct and examine the DOS below E_F in a-Si:H, as shown in figure 7(a). While the data are somewhat noisy due to numerical differentiation, the trends exhibited are sufficiently clear. As reported earlier, the density of deep states is increased by e- irradiation, and reduced by isochronal annealing. However these data also reveal systematic changes in the VB tail slope, plotted vs. annealing temperature in figure 7(b). The trend is quite similar to that observed in the TPC data plotted in figure 6(b), with a clear reduction in band tail slope occurring after anneals at 80°C and 120°C. The peak apparent in figure 7(a) above 1.6 eV is an artifact of strong optical absorption in the film ($\alpha t > 1$ invalidates the CPM assumptions).

3.4. Band tails, e-irradiation and Disorder

While an association between exponential band tails and disorder in bond lengths and angles in silicon thin films has long been accepted, understanding of the detailed linkage on an atomic scale is still developing. Computer modelling studies of amorphous silicon systems [33, 34] suggest that while tail states arise from a large number of atoms in the ensemble, there is a statistical (but not necessarily causal) association between short bonds and CB tail states, and long bonds and VB tail states.

For example Koch et al [35] demonstrate a clear correlation between increasing deposition temperature between 50°C and 150°C, and decreasing E_U. It is also known that film stress [36] and short and medium-range order [37], both linked to atomic structure, are dependent on growth

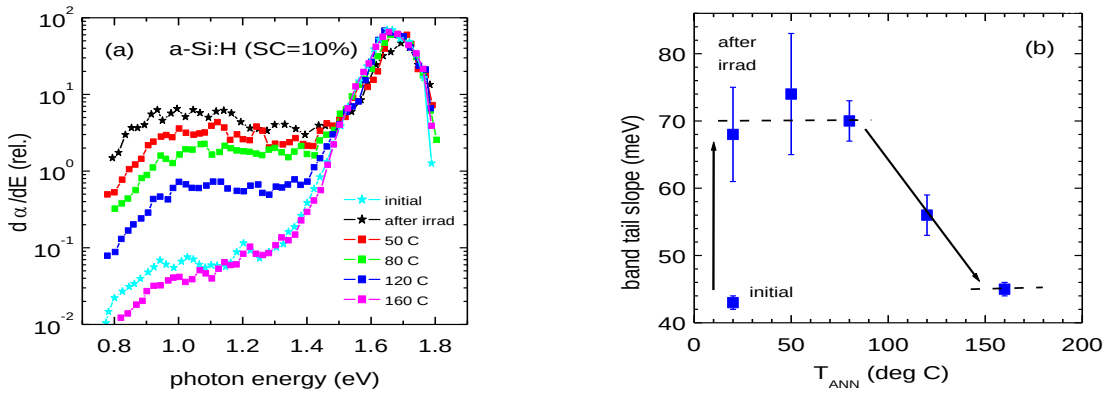

Figure 7. (a) DOS derived from CPM spectrum, (b) Characteristic VB tail energy calculated from best-fit lines to band tail regions, vs. annealing temperature.

conditions. Danesh et al [38] observed a correlation between E_U and the TO phonon frequency ω_{TO} obtained from Raman spectroscopy, and found a systematic reduction in E_U with increasing ω_{TO} which supports a linkage between steepening band tails and increased structural order.

There are reports of changes in structural order [39] and increases in volume [40] following light-soaking of a-Si:H samples, associated with structural changes in the lattice. In common with the SWE, and with e-irradiation induced changes in optical and electronic properties, these mechanical changes are also metastable, and samples may be thermally annealed back to, or close to, the as-deposited state.

The implication is therefore that e-irradiation results in reduced structural order, and further, that subsequent thermal annealing may improve or even restore the original degree of order to a-Si:H films. We have not yet carried out structure-sensitive measurements such as Raman spectroscopy or x-ray diffraction on e-irradiated samples. However, Köhler et al [41] have done so in the case of strongly light-soaked samples, which suggest changes in ω_{TO} tantalisingly close to the resolution limit. One may surmise that the e-irradiation regime used here is more aggressive than extensive light-soaking, given that up to 2 orders of magnitude more dangling-bond defects are created. These key experiments linking structural order and transport properties remain to be carried out.

3.5. Computer modelling of a-Si:H solar cells

Computer modelling enables material parameters to be incorporated into device structures and simulated to see if they might account for observed device behaviour. The 'inner workings' of the device are exposed, and may be used for more detailed analysis and to make informed suggestions for improvement. Modelling is thus a powerful tool in 'closing the loop' on structure-property relationships and performance optimisation. We modelled the a-Si:H device structure using *SC-Simul* [26, 27], and incorporated a range of defect densities and band tail slopes suggested by the above experiments to see if test results on e-irradiated cells can be reproduced. Material and device parameters are the default values used by *SC-Simul* except where otherwise stated. Summaries are given in figures 8 and 9. The experimental solar cell data is that presented in Astakhov et al [9].

The simulations in figure 8 were performed with band tail slopes of 25 meV (CB) and 50 meV (VB) to represent a 'typical' device, in which only the deep defect density is varied. It can be seen that the experimental data are reasonably well reproduced over a wide range of defect densities for both 0.3 μm and 1 μm absorber layers. The main discrepancy is with the value of V_{OC}, which is too low in the simulation. This may be due to a need to adjust the p- and n-layer simulation parameters, as the default settings were used here. The abrupt fall in V_{OC} for $N_S > 10^{17}$ cm^{-3} is also not reproduced, and remains a topic for future investigation.

The simulations in figure 9 represent our first attempt at modelling the effects of degradation of the

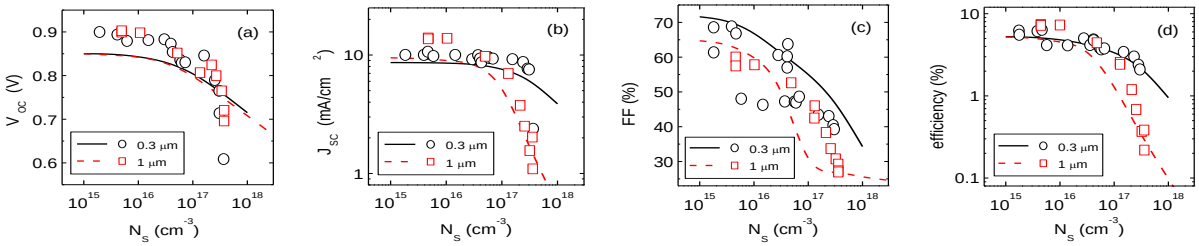

Figure 8. Effect of e-irradiation and subsequent annealing on PV parameters: (a) VOC, (b) JSC, (c) FF, (d) efficiency, measured for a-Si:H solar cells, with i-layer thicknesses of 0.3 μm and 1 μm. Lines are computer simulations obtained by changing defect density in line with experimental spin density.

band tails due to e-irradiation. The defect density is varied across a series of curves for band tail slopes encompassing those measured experimentally. Device performance is found from these simulations to be quite insensitive to the CB tail slope; and not much happens until it approaches the value of the VB tail slope. Thus what is shown in figure 9 is largely due to changes in VB tail slope. For an i-layer thickness of 0.3 μm, efficiency for $N_D < 3\times10^{16}$ cm^{-3} varies gradually with kT_V and roughly halves between 40 meV and 70 meV. For $N_D > 10^{17}$ cm^{-3} the curves coalesce, becoming independent of tail slope. For an i-layer thickness of 1 μm, behaviour is more complex for $N_D > 10^{17}$ cm^{-3}, with broader band tails predicted to actually increase efficiency. This may be due to a redistribution of charge between defects and tail states, which improves the electric field profile at some critical point in the device. This rather counter-intuitive result requires more detailed analysis of the model predictions.

Experimentally, we have no means of independently changing the band tail slopes by e-irradiation without simultaneously affecting the deep defect density, and indeed the two may be fundamentally inseparable [34]. According to the simulations, N_D needs to be below 10^{16} cm^{-3} to reliably distinguish the influence of the band tails on cell performance. This may be the case in modern device-quality material, as discussed by Liang et al [42] from a different perspective.

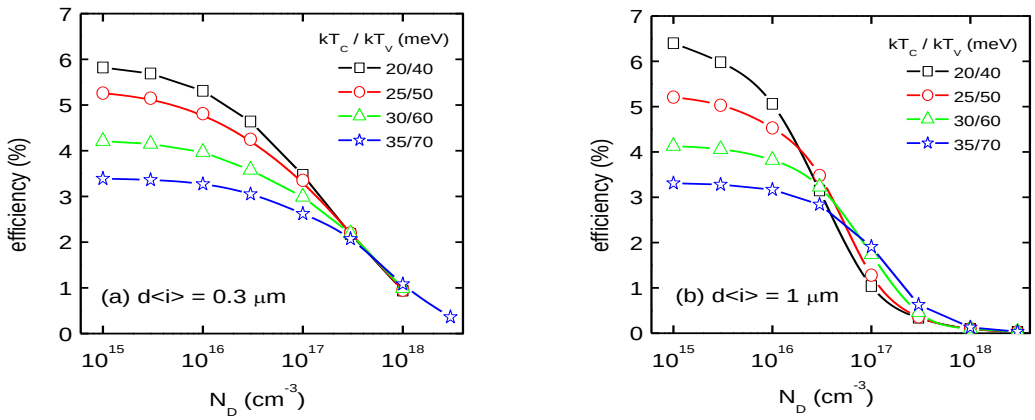

Figure 9. Simulated PV efficiency *vs.* defect density N_D for a range of band tail slopes, for i-layer thicknesses of (a) 0.3 μm, (b) 1 μm.

4. Conclusions

Hydrogenated amorphous and microcrystalline silicon thin films irradiated with 10^{17} electrons cm^{-2} contain a density of dangling-bond defects approaching 10^{18} cm^{-3}. These films have been investigated using the transient photocurrent method to measure the density of localised states above the Fermi level vs. energy depth. It is found that the deep DOS detected by TPC increases in keeping with the spin density following e-irradiation, and decreases in a similar way after isochronal thermal annealing

at progressively increasing temperatures. We have also observed changes in the conduction band-tail slope, which reaches a maximum value after e-irradiation of some 36 meV, compared with typically 20 to 22 meV in as-deposited samples. e-irradiated samples may be returned close to the as-deposited state following annealing at 180°C for 30 mins. The behaviour of the Urbach tail following e-irradiation has been reviewed, and evidence for proportionate changes in valence band tail slope is present. This reaches a value of some 70 meV after e-irradiation, and returns to the as-prepared value of 45 meV when fully annealed. The greatest reduction in slope occurs in both cases after annealing at around 120°C. Since band tail slopes are thought to be associated with the degree of disorder, we suggest that the doses of e-irradiation used here may be sufficient to bring about metastable changes in structural order in the amorphous 'lattice'. As the band-tail effects anneal in a way which mirrors that of deep defects, it is suggested that both may be linked by the action of mobile hydrogen in relieving strain in the structure, as a by-product of passivating dangling bonds. Since such high defect densities (and by inference, degree of disorder) cannot readily be generated by light-soaking these effects appear not to have been observed, or at least reported, previously. Natural variations in 'intrinsic' disorder, typically introduced by varying the material preparation conditions, can be correlated with the TO phonon peak in the Raman spectrum. However, detecting any additional disorder caused by light-soaking appears to be at the limit of such measurements. Because e-irradiation gives rise to one to two orders of magnitude more dangling bonds than standard light-soaking regimes, it seems possible that the hydrogen passivation of this larger density of metastable defects may be sufficient to enable a more definite connection between structural order and transport properties to be made in future.

Acknowledgments
The authors thank Charlie Main, Rudi Brüggemann and co-workers for their contributions over many years to the development of DOS spectroscopy and transport simulations. We are grateful to technical staff at IEK-5, Forschungszentrum Jülich who assisted in preparation and characterisation of samples, and to Florian Köhler and Christophe Longeaud for a number of most useful recent discussions.

References
[1] Srour J R, Palko J W, Lo D H, Liu S H, Mueller R L and Nocerino J C 2009 *IEEE Trans. Nucl. Sci.* **56** 3300
[2] Srour J R, Vendura G J, Lo D H, Toporow C M C, Dooley M, Nakano, R P and King E E 1998 *IEEE Trans. Nucl. Sci.* **45** 2624
[3] Wang K, Lord K, Woodyard J R 2000 *IEEE PV Specialists Conference* p 1057
[4] van Swaaij R A C M M and Klaver A 2008 *J. Non-Cryst. Solids* **354** 2464
[5] Kuendig J, Goetz M, Shah A, Gerlach L and Fernandez E 2003 *Sol. Energ. Mat. Sol. Cells* **79** 425
[6] Meillaud F, Vallat-Sauvain E, Niquille X, Dubey M, Shah A and Ballif C 2006 *J. Non-Cryst. Solids* **352** 1851
[7] Astakhov O, Smirnov V, Carius R, Petrusenko Yu, Borysenko V, Böttler W and Finger F 2012 *J. Non-Cryst. Solids* **358** 2198
[8] Smirnov V, Astakhov O, Carius R, Pieters B E, Petrusenko Yu, Borysenko V and Finger F 2012 *Appl. Phys. Lett.* **101** 143903
[9] Astakhov O, Smirnov V, Carius R, Pieters B E, Petrusenko Yu, Borysenko V and Finger F 2014 *Sol. Energ. Mat. Sol. Cells* **129** 17
[10] Smirnov V, Astakhov O, Carius R, Petrusenko Yu, Borysenko V and Finger F 2012 *Jpn. J. Appl. Phys.* **51** 022301
[11] Astakhov O, Carius R, Petrusenko Yu, Borysenko V, Barankov D, Finger F 2007 *Mat. Res. Soc. Symp. Proc.* **989** 3
[12] Astakhov O, Carius R, Finger F, Petrusenko Yu, Borysenko V and Barankov D 2009 *Phys. Rev. B* **79** 104205

[13] Liao N M, Li W, Liu Z, Jiang Y D, Ma N, Li Y, Wu Z M and Li S B 2008 *Phil. Mag. Lett.* **88** 871
[14] Brüggemann R, Bronner W and Mehring M 2001 *Sol. St. Commun.* **119** 23
[15] Bronner W, Mehring M and Brüggemann R 2002 *Phys. Rev.* B **65** 165212
[16] Bronner W, Kleider J P, Brüggemann R and Mehring M 2003 *Thin Solid Films* **427** 51
[17] Stutzmann M, Jackson W B and Tsai C C 1985 *Phys. Rev.* B **32** 23
[18] Stutzmann M, Rossi M C and Brandt M S 1994 *Phys. Rev.* B **50** 11592
[19] Reynolds S, Anand S, Meftah A and Smirnov V 2012 *J. Non-Cryst. Solids* **358** 2202
[20] Smirnov V, Das C, Melle T, Lambertz A, Hülsbeck M, Carius R, Finger F 2009 *Mater. Sci Eng.* B **159-160** 44
[21] Xiao J, Astakhov O and Finger F 2011 *Jpn. J. Appl. Phys.* **50** 071301
[22] Reynolds S, Main C, Webb D P and Rose M J 2000 *Philos. Mag.* **80** 547
[23] Main C 1997 *Mat. Res. Soc. Symp. Proc.* **143** 167
[24] Main C 2002 *J. Non-Cryst Solids* **299-302** 525
[25] Tiedje T, Cebulka J M, Morel D L and Abeles B 1981 *Phys. Rev. Lett.* **46** 1425
[26] M Rösch, PhD thesis (2003), Universität Oldenburg http://oops.uni-oldenburg.de/247/
[27] Brüggemann R and Rösch M 2005 *J. Optoel. Adv. Mater.* **7** 65
[28] Reynolds S, Smirnov V, Finger F, Main C and Carius R 2005 *J. Optoel. Adv. Mater.* **7** 91
[29] Kleider J P, Longeaud C, Brüggemann R and Houzé F 2001 *Thin Solid Films* **383** 57
[30] Longeaud C, Roy D and Teukam Hangouan Z 2000 *Appl. Phys. Lett.* **77** 3604
[31] Roy D, Longeaud C and Saadane O 2002 *J. Non-Cryst. Solids* **299-302** 511
[32] Pierz K, Mell H and Terukov J 1985 *J. Non-Cryst. Solids* **77–78** 547
[33] Fedders P A, Drabold D A and Nakhmanson S 1998 *Phys. Rev* B **58** 15264
[34] Khomyakov P A, Andreoni W, Afify N D and Curioni A 2011 *Phys. Rev. Lett.* **197** 255502
[35] Koch C, Ito M and Schubert M 2001 *Sol. Energ. Mat. Sol. Cells* **68** 227
[36] Tzanetakis P 2003 *Sol. Energ. Mat. Sol. Cells* **78** 369
[37] Köhler F, Zimmermann T, Muthmann S, Gordijn A and Carius R 2014 *IEEE J. Photovoltaics* **4** 4
[38] Danesh P, Toneva A, Savatinova I and Liarkapis E 1996 *J. Non-Cryst. Solids* **204** 265
[39] Gupta S, Katiyar R S, Weisz S Z and Balberg I 2000 *J. Non-Cryst Solids* **266-269** 496
[40] Nonomura S, Yoshida N, Gotoh T, Sakamoto T, Kondo M, Matsuda A and Nitta S 2000 *J. Non-Cryst. Solids* **266-269** 474
[41] Köhler F, private communication
[42] Liang J, Schiff E A, Guha S, Yan B and Yang J 2006 *Appl. Phys. Lett.* **88** 063512